Supplementary Information

Perilipin 5 mediated lipid droplet remodelling revealed by coherent Raman imaging

Nils Billecke[a], Madeleen Bosma[b,+], William Rock[a], F. Fleissner[a], G. Best[a], Patrick Schrauwen[b], Sander Kersten[d], Mischa Bonn[a], Matthijs K. C. Hesselink[c,*], and Sapun H. Parekh[a,*]

_____

[a]Molecular Spectroscopy Department, Max Plank Institute for Polymer Research, Ackermannweg 10, 55128 Mainz, Germany

[b]Departments of Human Biology and [c]Movement Sciences, School for Nutrition, Toxicology and Metabolism, Maastricht University Medical Center, 6200 MD Maastricht, The Netherlands

[d]Nutrition, Metabolism and Genomics Group, Division of Human Nutrition, Wageningen University, 6700EV Wageningen, The Netherlands

[+]Current Address: Department of Cell and Molecular Biology, Karolinska Institutet, P.O. Box 285 SE-171 77 Stockholm, Sweden

[*]Corresponding Authors:

Matthijs K. C. Hesselink, Tel: + 31433881317, Email: matthijs.hesselink@maastrichtuniversity.nl

Sapun H. Parekh, Tel: +496131379326, Email: parekh@mpip-mainz.mpg.de

Image creation and processing

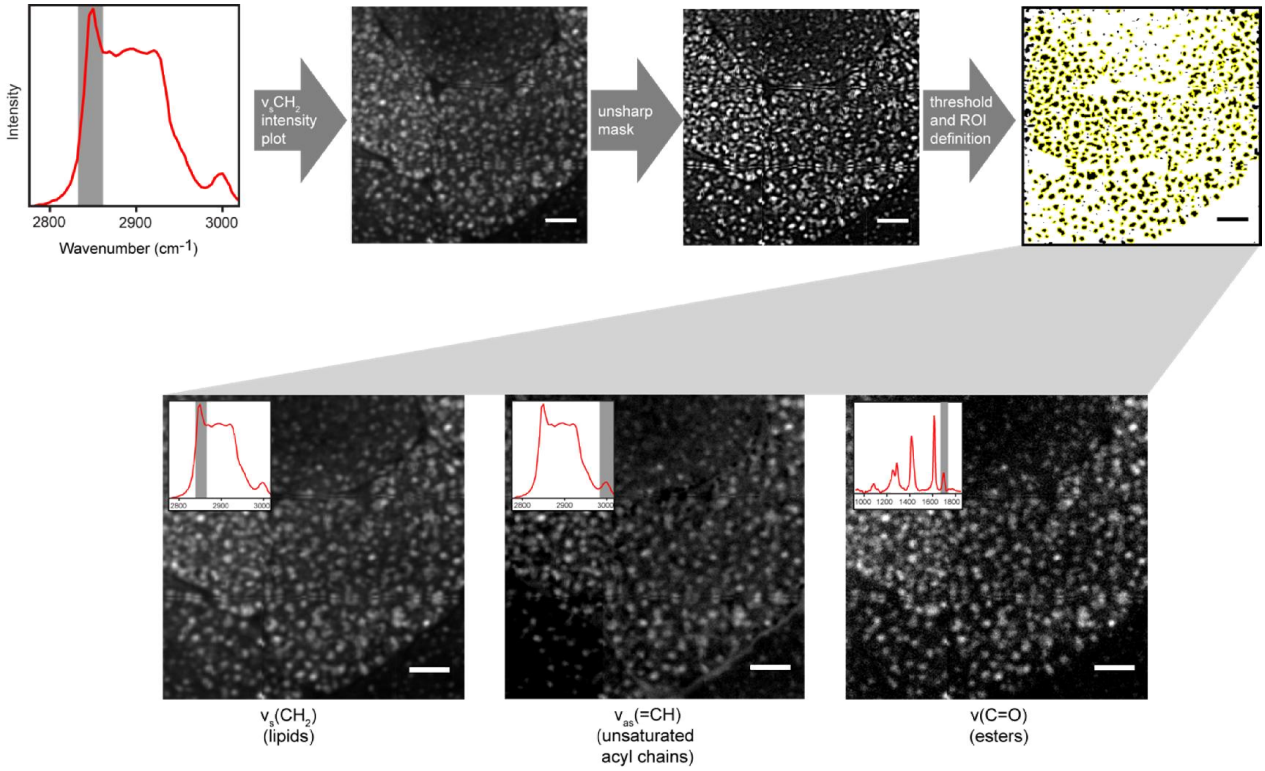

Supplementary Figure I: Flowchart of image creation process and determination of ROI identification for individual LDs within samples (here rat tibialis tissue section). Scale bar is 10 µm.

All collected raw hyperspectral datasets were post-processed according to the modified Kramers-Kronig algorithm (1) to retrieve the resonant part of the CARS signal referred to as the Raman-like CARS (RL CARS) spectrum. The RL CARS spectra, which are linear in concentration, were then used to plot the integrated intensities of the CH_2 symmetric vibrations (2840-2856 cm^{-1}) in the sample as 2D images using IgorPro 6.22A. These raw images were exported to ImageJ to identify lipid droplets and created a region of interest using the ImageJ unsharp mask tool. Settings were adjusted depending on the respective sample between 1.0 and 2.0 pixel radius, where the mask weight was kept at 0.9. From the weighted images, a binary image was created using the thresh-holding function. ImageJ watershed function was used to distinguish between LDs localized in clusters. ROI were then superimposed on the raw CH_2 images and checked for correct ROI definition. Particle sizes were then measured (ImageJ particle analysis). For different vibrational modes, additional 2D images of intensities of ester bonds (C=O stretching from 1730-

1750 cm^{-1}) and the asymmetric =CH vibration (3001-3018 cm^{-1}) were plotted for each sample. The pre-defined ROIs were then superimposed on each image plot of the respective sample, and mean gray values were measured using ImageJ. The obtained dataset contained the size, relative localization and mean intensities for all above mentioned molecular vibrations for each individual LD in the sample. The data matrices were then exported to OriginPro for statistical analysis.

Linear correlation between measured and actual object size using monodisperse polystyrene microbeads

Below we present calibration data using RL CARS vibrational images to size and compute the =CH concentration of near-diffraction limited and larger polystyrene spheres. The plots shows that the measured polystyrene bead size increases linearly with diameter while the total signal increases with area, as predicted. This verifies that our size determination and chemical quantification of LDs is robust for the object sizes measured in this study.

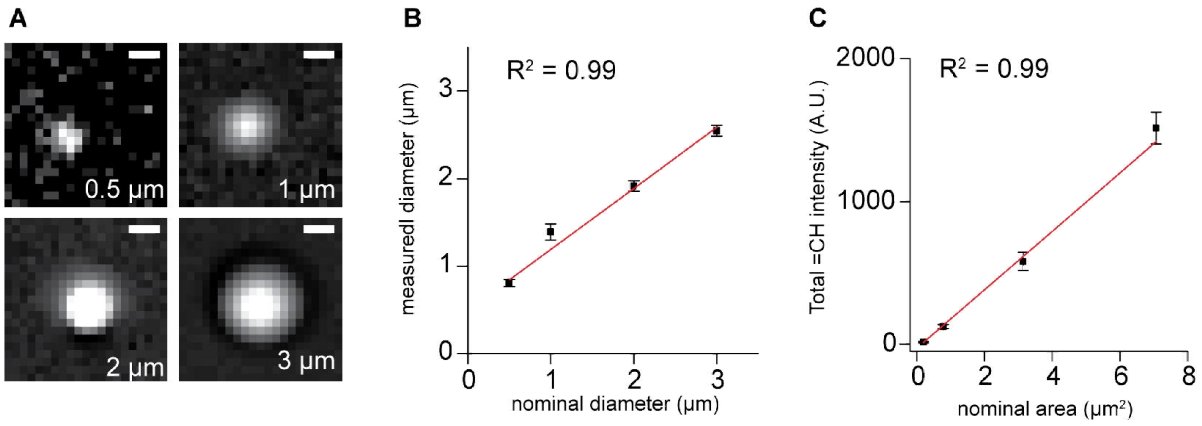

Supplementary Figure II: (A) Images of the broad =CH band of polystyrene (3005-3060 cm-1) obtained from polystyrene beads embedded in agarose and imaged by broadband CARS. Data were linearized identically as described in the main text. **(B)** Measured vs. actual (manufacturer) values for bead diameter determined using analogous thresholding to that for LD size analysis. **(C)** Total=CH intensities scales linearly with plotted microbead area in the results section (Fig. 3). N = 4 beads per measurement; error bars are SD; scale bar = 1 µm.

Lipid-loading in C2C12 myotubes

Whole cell images of lipid loading in differentiated myotubes transfected with GFP-PLIN5. Lipid droplets are seen in phase contrast microscopy and are co-localized with a rim of GFP-PLIN5.

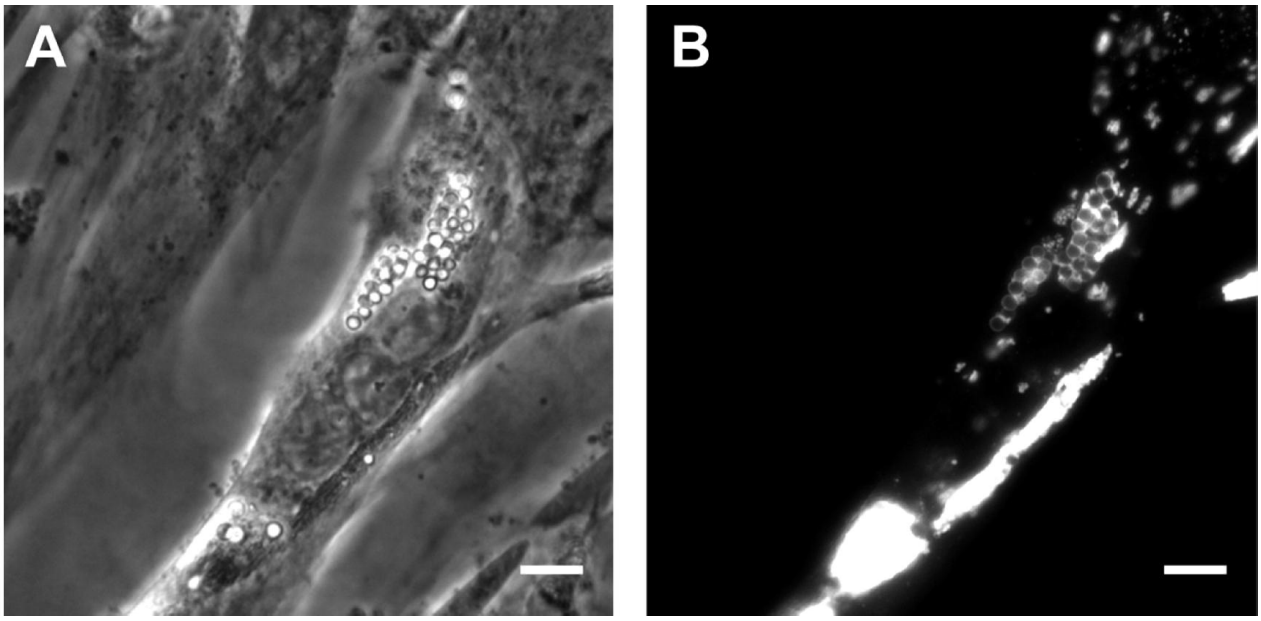

Supplementary Figure III: (A) Phase-contrast image of differentiated C2C12 myotube after PLIN5-GFP transfection and 20μM fatty acid incubation (oleate:palmitate = 3:1) show bright LDs in the cytoplasm of the fiber. **(B)** Corresponding fluorescence image confirms the ectopic PLIN5 expression, LDs are clearly decorated with PLIN5-GFP. Scale bars are 20 μm.

Quantitative determination of unsaturation from =CH vibration

Lipid unsaturation can be determined using the C=C vibration at 1650 cm^{-1} or the =CH vibration between 2985 cm^{-1} and 3022 cm^{-1}. The C=C vibration is most commonly used, but can be convoluted by the strong amide I peak from proteins, especially in cells and tissues. Therefore we chose to use the =CH vibration for unsaturated carbon quantification.

As verification of this metric, we show that the ratio of integrated intensities of =CH:CH_2 of RL CARS spectra for increasing molar fractions of the monounsaturated oleic acid exhibits a linear dependency. The offset of the linear fit of the peak ratios can be attributed to asymmetric CH_3 vibrations (2960 cm^{-1} – 2970 cm^{-1}), whose shoulder reaches into the =CH vibrational peak. Regardless, the molar ratio of =CH to total CH_2 content is correctly reflected in the intensity ratio and hence is a valid measure of (un)saturation of lipid species in our model.

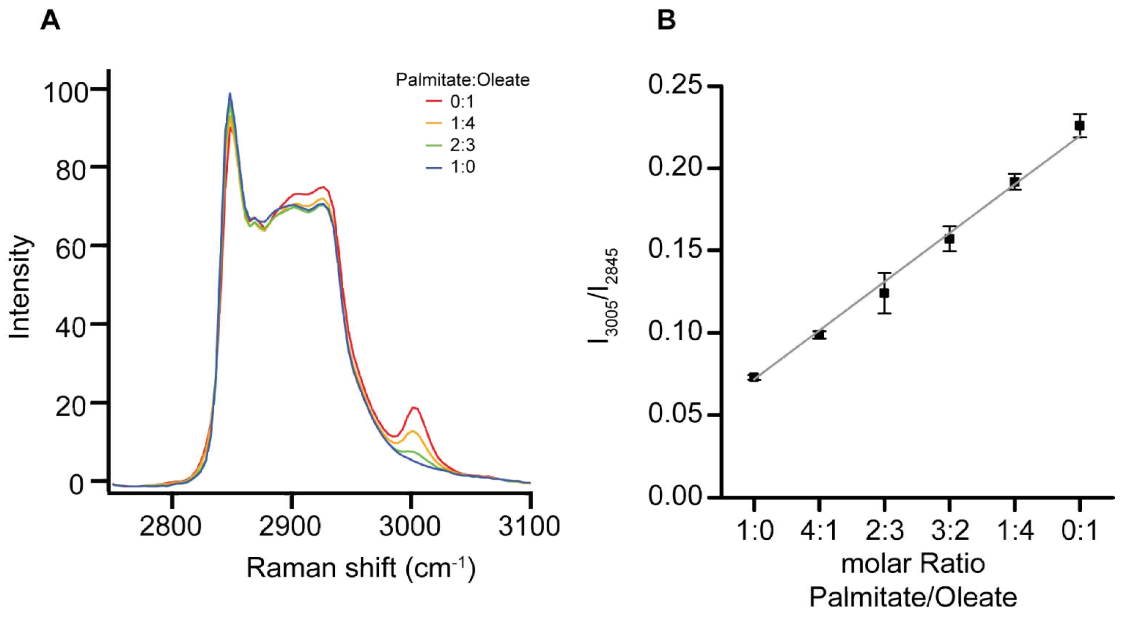

Supplementary Figure IV: (A) Spectra of 1 M fatty acid mixtures with varying amounts of palmitate and oleate at indicated molar fractions in deuterated DMSO. **(B)** Ratios of integrated peak intensities of =CH:CH_2 vibrations (I_{3005}/I_{2852}) show the linear dependency of level of unsaturation in the mixture. N = 3 separate measurements per composition; error bars are SD.

Correlative imaging of CH_2 CARS images and Bodipy labeled LDs in the same tissue section

Correlative imaging of control tibialis muscle demonstrates that CH_2 CARS images correlate well with wide-field fluorescence morphology from LDs stained with lipophilic Bodipy 493 dye from the same tissue section after CARS imaging. This shows that CH_2 intense regions in native tissue accurately reflect areas of augmented of lipid content. The spectra from LDs and sarcoplasm are distinctly different, and the fingerprint region from the LD shows, within the signal-to-noise of the measurement, a surprising absence of ester bonds.

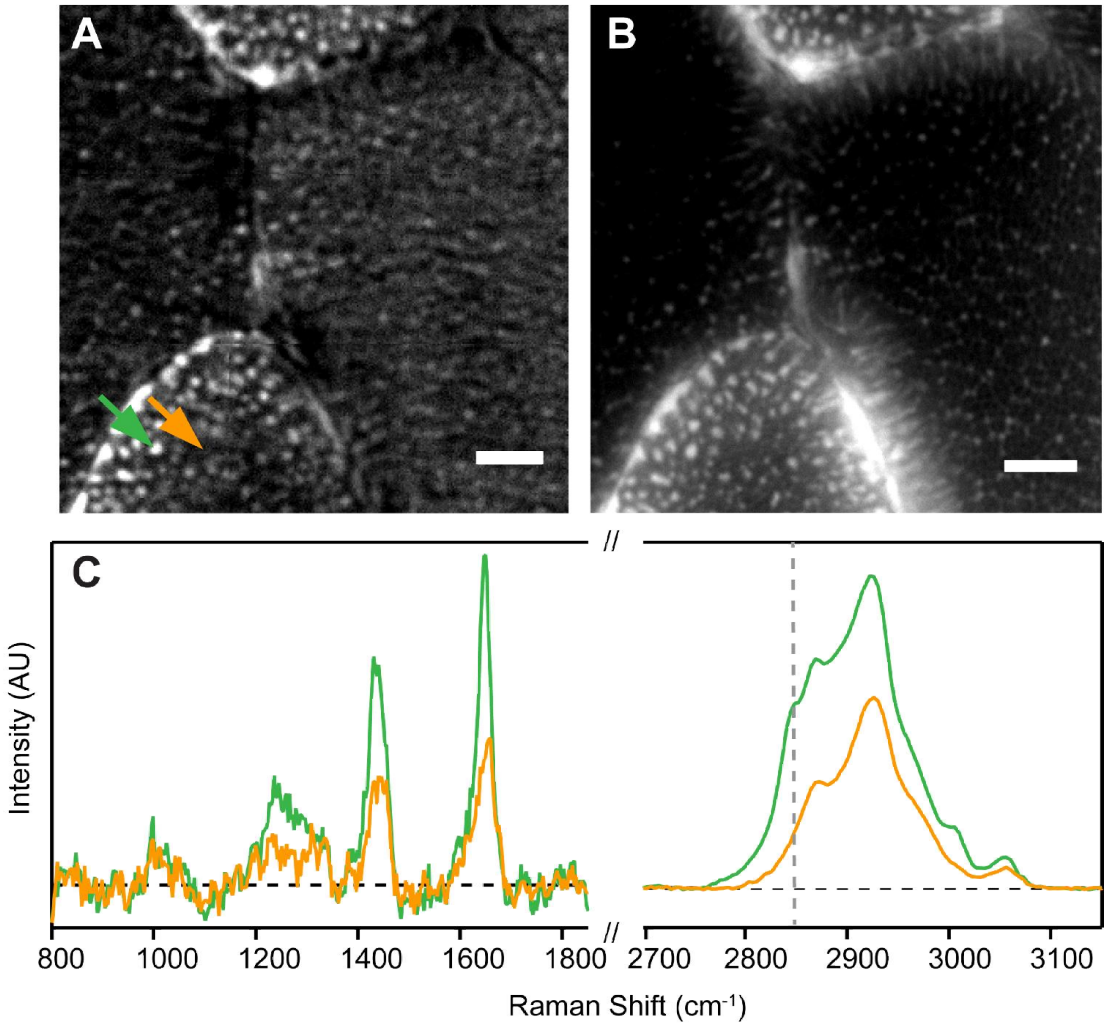

Supplementary Figure V: (A) CH_2 intensity image showing small lipid droplets in control rat tibialis muscle. **(B)** Bodipy 493/503 histochemical micrograph of the same tissue showing LDs equivalent to the CARS image. **(C)**Spectra from inside a LD (green)) show the appearance of bands at ~ 2845 cm^{-1} and ~3005cm^{-1} specific to lipids. Spectrum of a region in the sarcolemma (yellow) is void of these bands. Scale bar is 10 µm.

RL CARS spectra of lipid droplets and surrounding cytoplasm/sarcoplasm upon PLIN5 overexpression

The RL CARS spectrum of the cytoplasm of differentiated C2C12 myotubes and sarcoplasm tibialis muscle both overexpressing PLIN5 show virtually no ester contribution outside of LDs. The blue spectra clearly show no peak from 1730 – 1750 cm^{-1}.

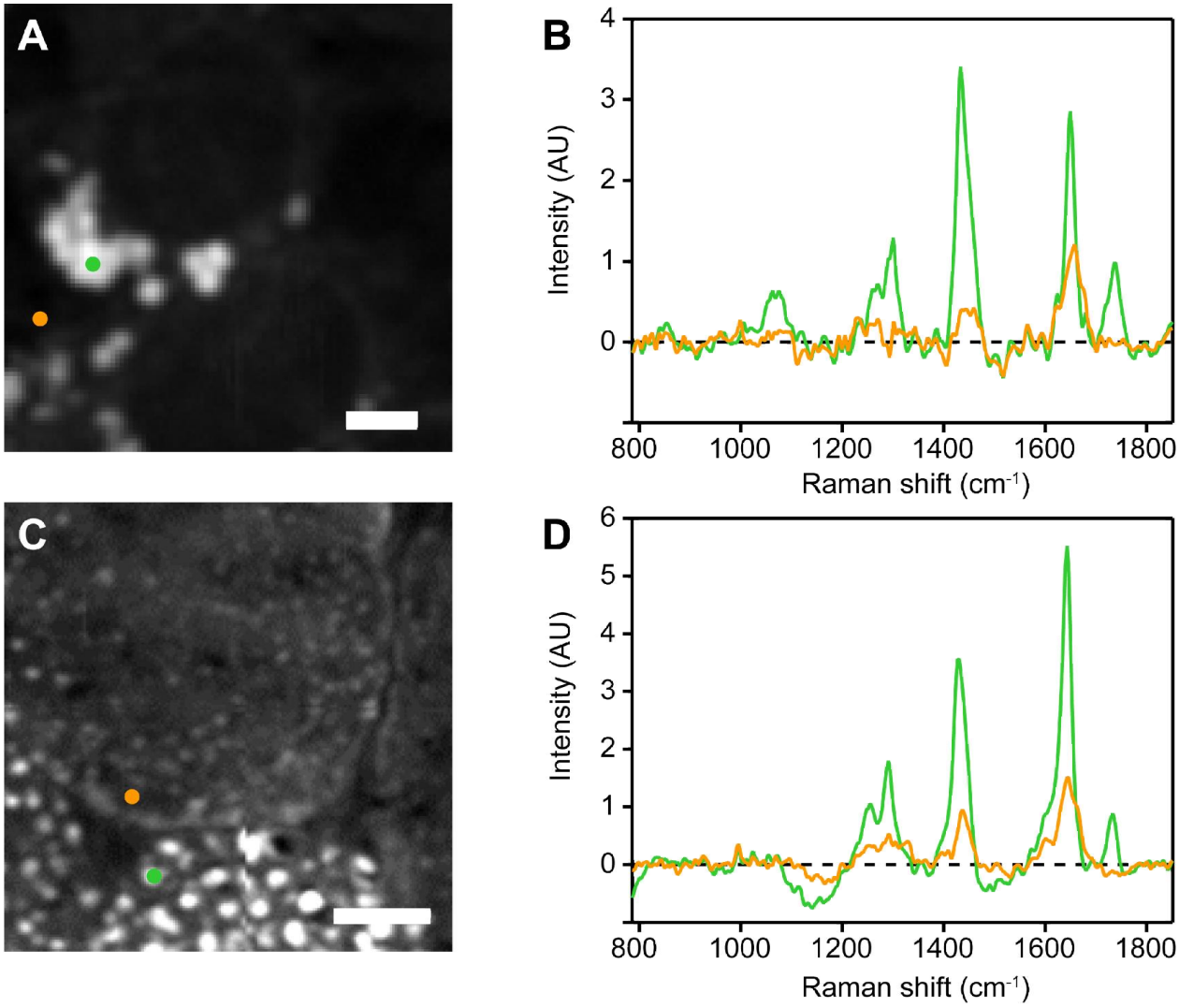

Supplementary Figure VI: (A) CH_2 intensity images show enlarged lipid droplets in PLIN5 overexpressing C2C12 myotubes and **(C)** rat tibialis muscle. **(B)**, **(D)** Representative spectra of LDs (red) in comparison to LD-free cytoplasm and sarcoplasm (blue). Scale bar is **(A)** 5 µm and **(C)** 20 µm. Note the presence and absence, respectively, of the band associated with ester bonds (C=O stretching from 1730-1750 cm^{-1}) in LDs and LD-free cytoplasm and sarcoplasm.

Genetic and protein changes in accompanying PLIN5 overexpression

Quantitative PCR was performed on tibialis muscle sections by extracting RNA from the central regions of tissue sections to maximize the proportion of cells successfully transfected with PLIN5. This was done to minimize the mixture of the non-transfected cells with the transfected cells for the genetic analysis and highlight potentially small differences in gene expression. From this transcriptional analysis, we observed that diacylglycerol O-acyltransferase homolog 1 (DGAT1) was significantly increased by 260% upon PLIN5 overexpression (Supplementary Fig. VII A). Similar sample segregation was not possible in differentiated C2C12 myotubes, which led to substantial mixing of non-transfected and transfected cells in the lysate, so qPCR on mRNA would not provide us with useful information on these samples.

We further attempted to quantify changes in DGAT1 at the protein level in the samples. PLIN5 overexpressing C2C12 myotubes exhibited 30% more DGAT1 immunofluorescence than control myotubes (Supplementary Fig. VII B). Similar immunofluorescence staining did not show reliable staining in tissue samples despite numerous attempts with different fixation protocols, primary antibodies, and secondary antibodies. Despite a statistically significant increase in DGAT1 gene expression in muscle tissue and DGAT1 immunofluorescence in muscle cells upon PLIN5 overexpression (Supplementary Fig. V), we were unable to globally detect changes in DGAT1 protein levels via immunoblot analysis. This apparent discrepancy can be explained by considering the following: 1) DGAT1 gene expression changes in tibialis muscle were evaluated in geometrical locations (center region) of the tissue sections with most effective PLIN5 transfection and 2) DGAT1 protein level in differentiated C2C12 myotubes was measured at the single-cell level. This is in contrast to the immunoblot analysis that used whole muscle cell or tissue lysates.

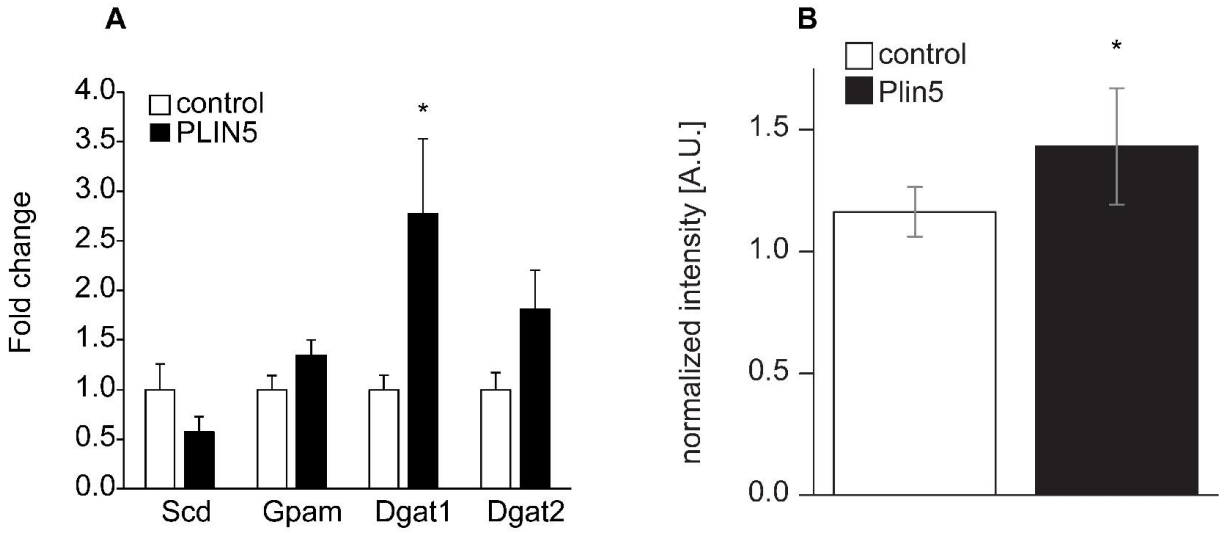

Supplementary Figure VII: (A) PLIN5 overexpression leads to increased transcription levels of diacylglycerol O-acyltransferase homolog 1 (*Dgat1*) in electroporated tibialis muscle. N = 6 PLIN5 overexpressing tissue sections and N = 7 control tissue sections. Error bars are SEM, and * denotes $p < 0.05$. **(B)** DGAT1 immunofluorescence increases in differentiated C2C12 myotubes with PLIN5 overexpression. Normalized average fluorescence from 10 control and 10 PLIN5 overexpressing cells within the same field-of-view were compared. Error bars are SD and * denotes $p < 0.05$.

Supplementary Materials and Methods

Quantitative determination of unsaturation in fatty acid mixtures

Oleic acid and palmitic acid (Sigma Aldrich) were solubilized in fully deuterated DMSO (Carl Roth, Karlsruhe, Germany) at 1M concentration and mixed at different ratios as indicated. Fatty acid mixtures were then measured under standard sample conditions as previously described. Raw CARS spectra were treated equivalent to the biological samples and intensity ratios calculated using IgorPro, ImageJ and Origin.

Preparation and BB-CARS imaging of monodisperse polystyrene microbeads

Gels of 5% agarose (Roth) in DI-water were prepared and polystyrene microbeads (Polyscience) of 0.5-3µm diameter were added at final dilutions of 1:100. The gels were then cast between two microscope cover slips and sealed with nail polish. To determine the bead size in CARS, hyperspectral images of microbead samples were acquired with a lateral pixel size of 0.2µm and a vertical pixel size of 0.3µm. Data processing was performed as described in the main text.

Quantitative PCR

Quantitative PCR (qPCR) was performed using SensiMix (Bioline, GC biotech, Alphen aan den Rijn) and a CFX384 Real-Time PCR Detection System (Bio-Rad). RNA was isolated as described previous (2). Primer sequences were derived from the Harvard PrimerBank and synthesized by Eurogentec (Eurogentec S.A.). Primer sequences are listed in Supplementary Table 1. Normalization was performed using the expression of 36b4.

Gene	Nucleotide Sequence
Scd Forward	AAGATATCCACGACCCCAGCTA
Scd Reverse	TGCAGCAGGGCCATGAG
Gpam Forward	GTCCAAAGCCATCCAGAAAG
Gpam Reverse	GAAACAAGAGCGGCAGATTC
Dgat1 Forward	TACTATCCAGAACTCCAT
Dgat1 Reverse	AGCCAATAGAAGAAGATG
Dgat2 Forward	TTAATCCTCTTCGCTCTA
Dgat2 Reverse	GATGTTATCTACCACTCTC

Supplementary Table I. Primer sequences for qPCR analysis of rat tibialis muscle transcription levels.

DGAT1 immunofluorescence

Immunofluorescence for DGAT1 was done using the same protocol as outlined in the main text. Briefly, cell were fixed in 4% PFA in PBS prior to incubation for 1 hour with rabbit anti-DGAT1 (PA1-16985; Thermo Fisher) diluted (1:20) in antibody dilution buffer (AbDil, 150 mM NaCl, 20mM Tris, 0.1 % NaN_3, 2% BSA at pH 7.4). After one washing step with AbDil and two washing steps with PBS, sections were stained with Cy5 goat anti-rabbit IgG secondary antibody (Life Technologies) in diluted 1:200 AbDil for 1 hour. Following one washing step with AbDil and two washing steps with PBS, sections were mounted in fluorescence mounting medium (Dako, Glostrup). Fluorescence and phase contrast images were acquired on an IX81 inverted microscope (Olympus) using Cell F imaging software. Fluorescent images were acquired for GFP-PLIN5 and DGAT1, and those cells which showed GFP-signals were marked as positive for PLIN5-overexpression. Average Cy5 fluorescence intensity in GFP-PLIN5 positive cells in 10 random fields of view, from two different transfections, were compared against corresponding average Cy5 fluorescence from non-transfected cells in the same field of view. These average fluorescence intensities were further normalized against bare regions in the same field of view to allow pooling of all the data.

References

1. Liu Y, Lee YJ, & Cicerone MT (2009) Broadband CARS spectral phase retrieval using a time-domain Kramers-Kronig transform. *Opt Lett* 34(9):1363-1365.
2. Bosma M*, et al.* (2013) Overexpression of PLIN5 in skeletal muscle promotes oxidative gene expression and intramyocellular lipid content without compromising insulin sensitivity. *Biochimica et biophysica acta*.